Electronic Supplementary Material (ESI) for Journal of Materials Chemistry C.

Supporting Information

Chiral deformation reversal of liquid crystal polymer actuators

Yaoyu Xiao, Zhichao Jiang, Lu Yin, Jie Jiang, Yue Zhao*

Département de Chimie, Université de Sherbrooke, Sherbrooke, Québec J1K 2R1, Canada

* Email: yue.zhao@usherbrooke.ca

Supplementary Figures

Actuation mechanism of LCN actuators

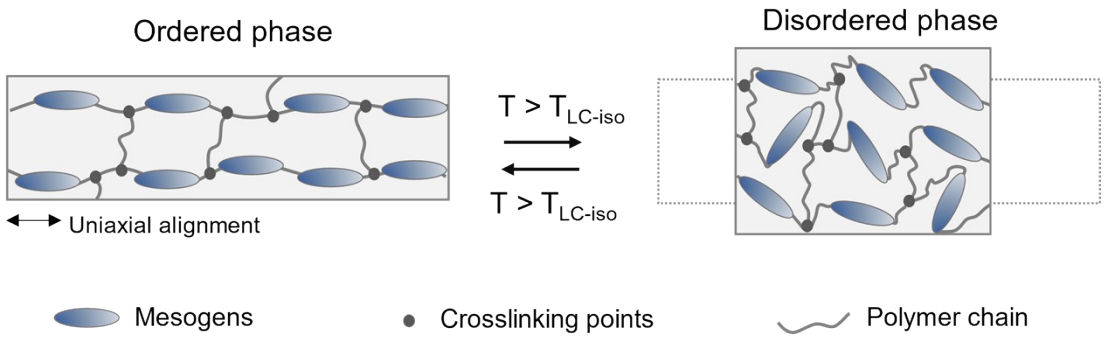

Fig. S1. Schematics showing the actuation mechanism of a monodomain main chain LCN actuator.

Discussion

Taking a monodomain main-chain LCN as an example, it contains uniaxially aligned mesogens and can display contraction/extension along the alignment direction upon heating/cooling. When the temperature (T) is above the LC-isotropic phase transition temperature (T_{LC-iso}), the order of the aligned mesogens is lost which causes a polymer chain conformation change from prolate to random coil due to the entropy elasticity of the polymer network. As a result, the LCN contracts uniaxially along the alignment direction when heated into the isotropic phase. When cooling to $T<T_{LC-iso}$, the order of the mesogens restores due to the memory effect from the crosslinked network. The concomitant random coil to prolate chain conformation changes lead to an elongation along the alignment direction. As such, the reversible order-disorder phase transition drives the macroscopic deformation of the LCN actuators.

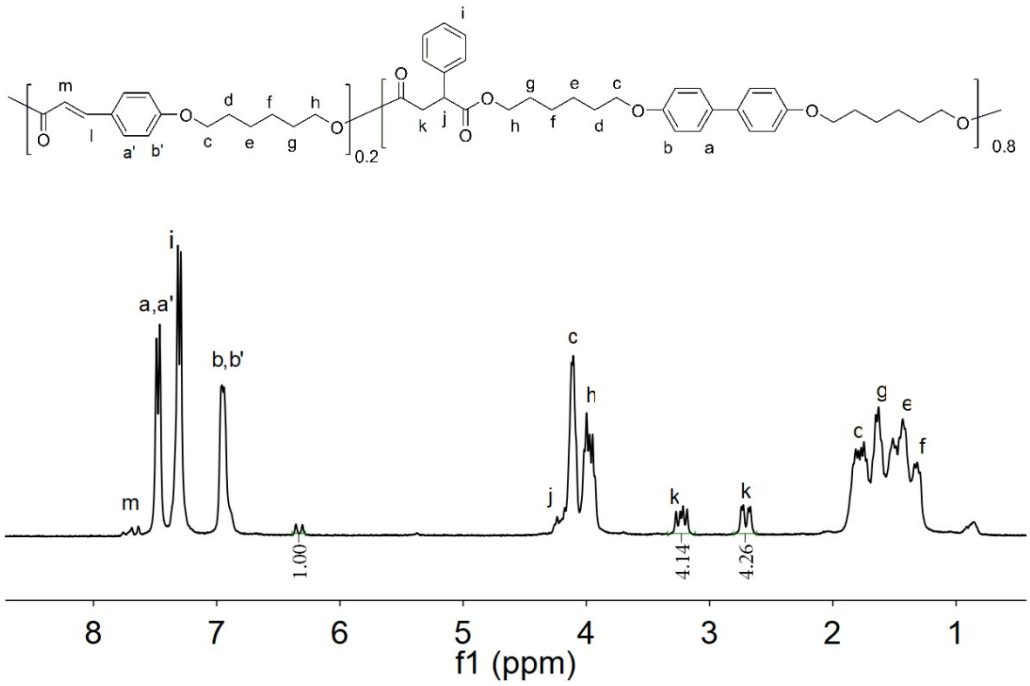

Fig. S2. ^{1}H NMR spectrum of LCP in $CDCl_3$.

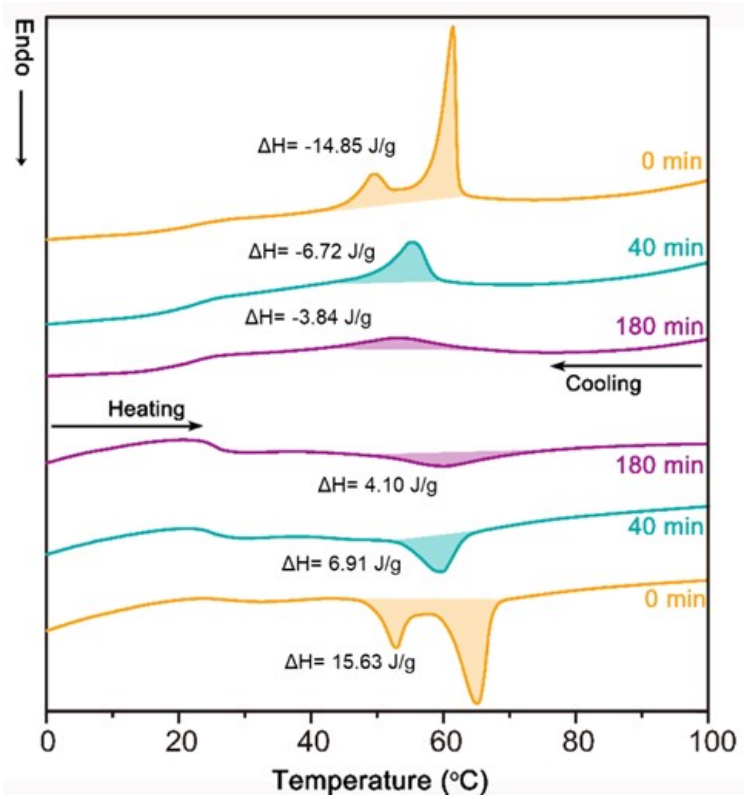

Fig. S3. Differential scanning calorimetry (DSC) curves of the LCN strips with each side photocrosslinked for 0 min (yellow), 40 min (green), and 180 min (purple), recorded in the second heating scan (bottom) and first cooling scan (top). For the two photocrosslinked samples, the draw ratio is 400%.

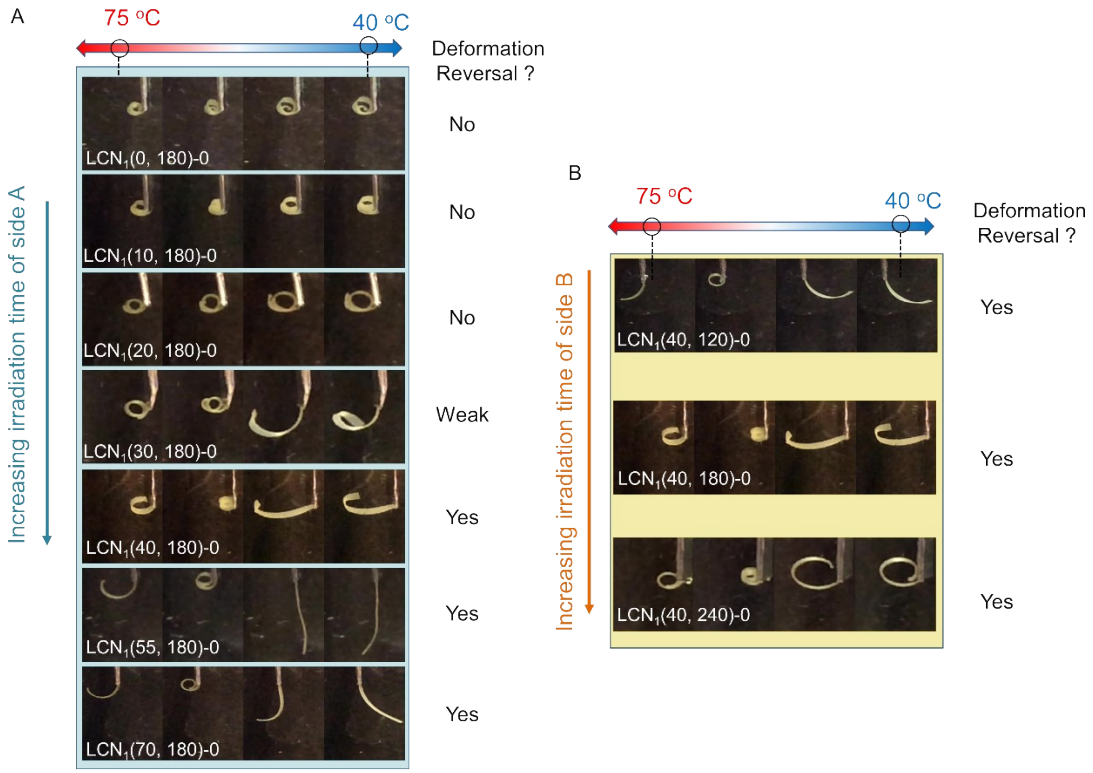

Fig. S4. Photographs showing bending behavior of $LCN_1(t_A,t_B)$-0 with (A) different crosslinking time of side A (represented by X) while crosslinking time of side B (represented by Y) is fixed as 180 min and (B) different crosslinking time of side B while crosslinking time of side A is fixed as 40 min for all samples during cooling from 75 °C to 40 °C. The dimensions of the samples are 7 (l) x 0.5 (w) x 0.07 (t) mm^3 in their maximum extended state.

Discussion

Fixing the crosslinking time of side B (t_B) to 180 min (light used: 320 nm, 180 mW. cm^{-2}) while varying the crosslinking time of side A (t_A), we observed a significant deformation reversal behavior when $t_A \geq 40$ min. Specifically, the strip curved toward the side A in isotropic phase. Upon cooling, the bending direction was first toward the lightly crosslinked side A and then reversed to the highly crosslinked side B, accompanied by a film elongation of ~50%. As t_A increased from 40 min to 70 min, all the films exhibited obvious deformation reversal behavior, but the film with higher t_A formed a straighter (less curved) shape at the same actuation temperature because of the reduced difference in crosslinking on both sides. Conversely, maintaining t_A at 40

min and increasing t_B from 120 min to 240 min, tighter coils bent toward the lightly crosslinked side A were formed at the same temperature during deformation reversal actuation process, which is caused by the enlarged crosslinking difference on both sides. Consistent with our previous research, the trends shown above are mainly caused by the different response temperatures and strains of the two sides with different crosslinking times: during cooling, the highly crosslinked side B tends to extend first at a higher temperature and thus the film bends toward side A; continuing to cool down, the lightly crosslinked side A begins to elongate significantly, causing the bending direction to reverse. In parallel, when heated, side A contracts at a lower temperature and causes it to bend to side A first; upon further heating, the highly crosslinked side B shrinks more so that the bending direction reverses to side B.

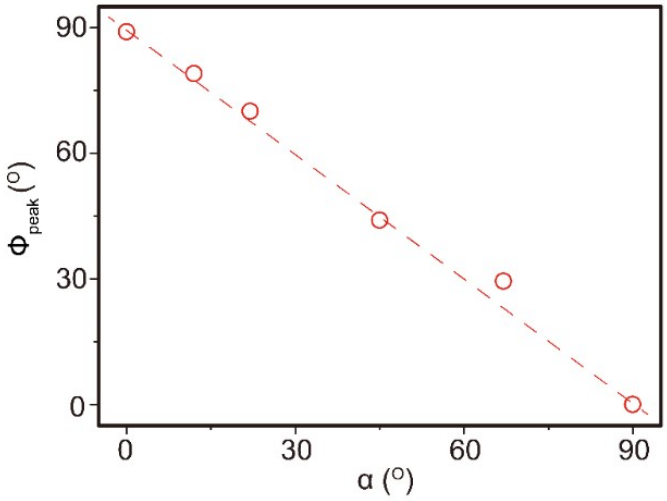

Fig. S5. Angular offset (α) plotted against the peak (the one within 0°-90°) in azimuthal diffraction profile shown in Fig. 2d. The y=x trend line is drawn to guide the eyes.

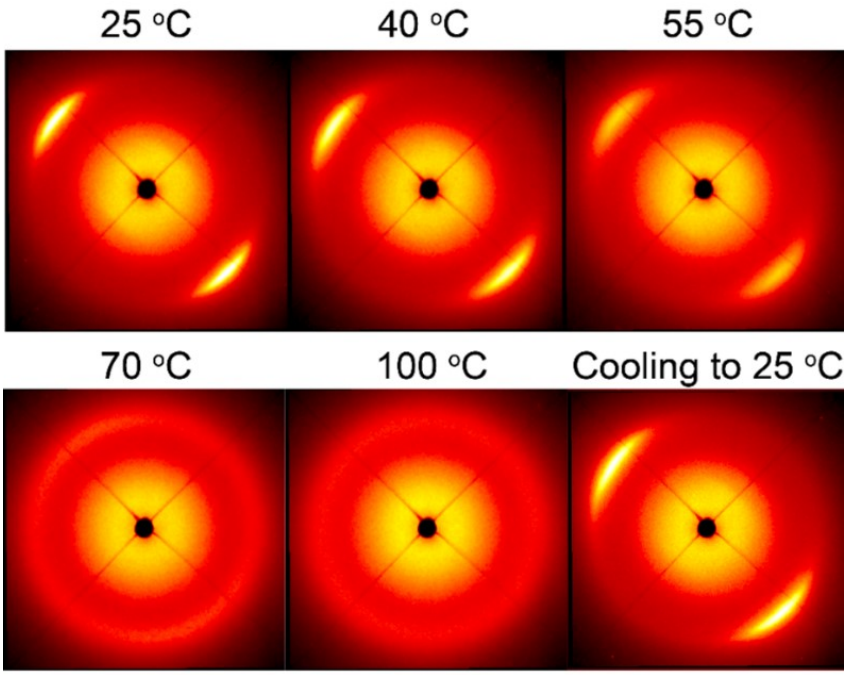

Fig. S6. Two-dimensional XRD patterns of monodomian LCN_1(40,180)-45 at different temperatures on heating from 25 °C to 100 °C and cooling to 25°C

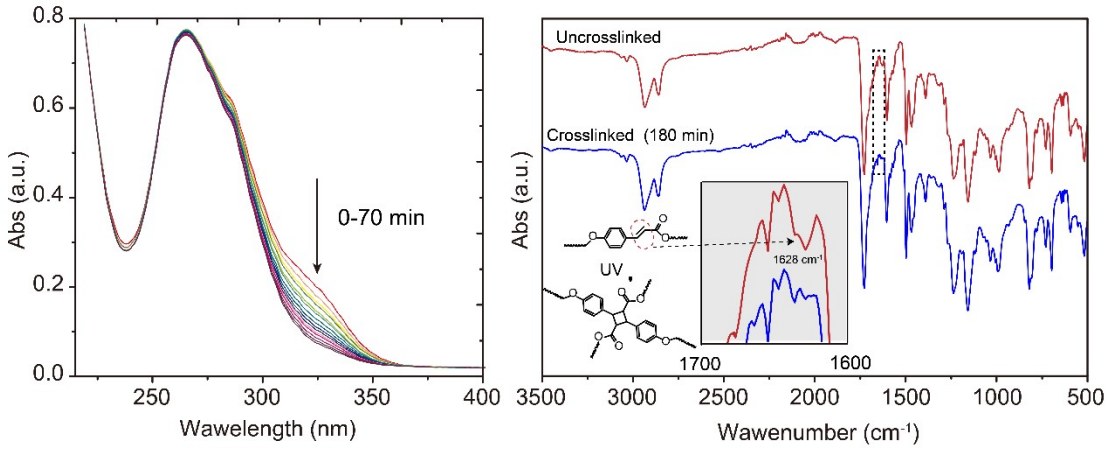

Fig. S7. Left: UV-Vis absorption spectra of a liquid crystal polymer film spin-coated on quartz with different UV-crosslinking times (320 nm, 30 mW/cm^2). Right: ATR-FTIR spectra of a stretched liquid crystal polymer film (ca. 0.07 mm) before and after 180 min UV-irradiation (320 nm, 180 mW/cm^2).

Discussion

UV-Vis absorption spectra of a thin liquid crystal polymer coating on quartz were monitored to verify the increasing crosslinking degree with the increase of

photocrosslinking time. As can be seen, the absorption peak at 325 nm decreases over UV irradiation time, implying the increase in the photodimerization degree of cinnamyl groups in the polymer film. In addition, ATR-FTIR spectra also confirm the successful photodimerization of cinnamyl groups. The peak at 1628 cm^{-1} for the uncrosslinked film sample, which is assigned to the stretching vibration ν(C=C) in the cinnamyl groups,[S1] become much weaker after being exposed to 180 min of UV irradiation (320 nm, 180 mW/cm^2).

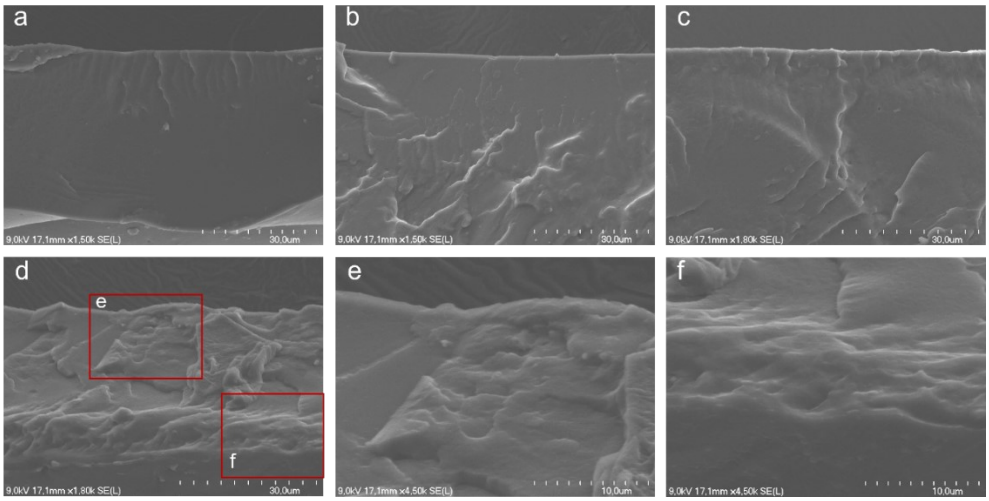

Fig. S8. SEM cross-sectional images for (a) LCN_1(40,180), (b) LCN_1(40,40), (c) LCN_1(70,70), (d) (e) and (f) LCN_1(180,180). Note: the samples were treated in chloroform at 40 °C for 12 h to remove the uncrosslinked parts before drying at room temperature for three days.

Discussion

From the SEM images of samples, including the LCN_1(40,40), LCN_1(70,70), LCN_1(180,180) and LCN_1(40,180), we cannot clearly distinguish their crosslinking differences. All samples showed solid cross-sections, indicating that there were no obvious non-crosslinked regions that were detectable under the experimental conditions we used. However, their crosslinking densities are different: the gel fractions of LCN_1(40,40), LCN_1(70,70), LCN_1(180,180) are 47%, 74% and 91%, respectively.

Moreover, although hard to be detected, a crosslinking gradient is expected to exist within the asymmetrically crosslinked LCNs.

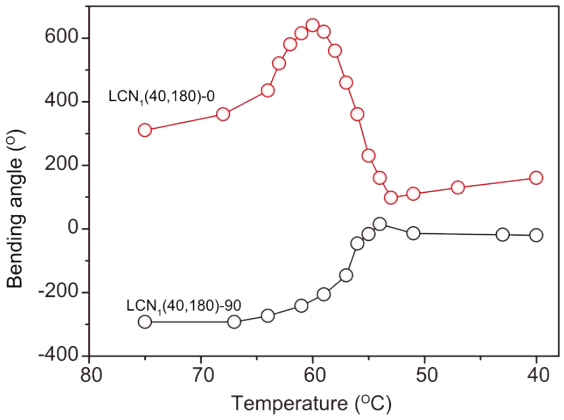

Fig. S9. Bending angle change as a function of temperature for LCN_1(40,180)-0 and LCN_1(40,180)-90. Here, a bending angle of the film curling toward the side crosslinked for 40 min (side A) is defined as positive, while that of the film curling toward side B is defined as negative.

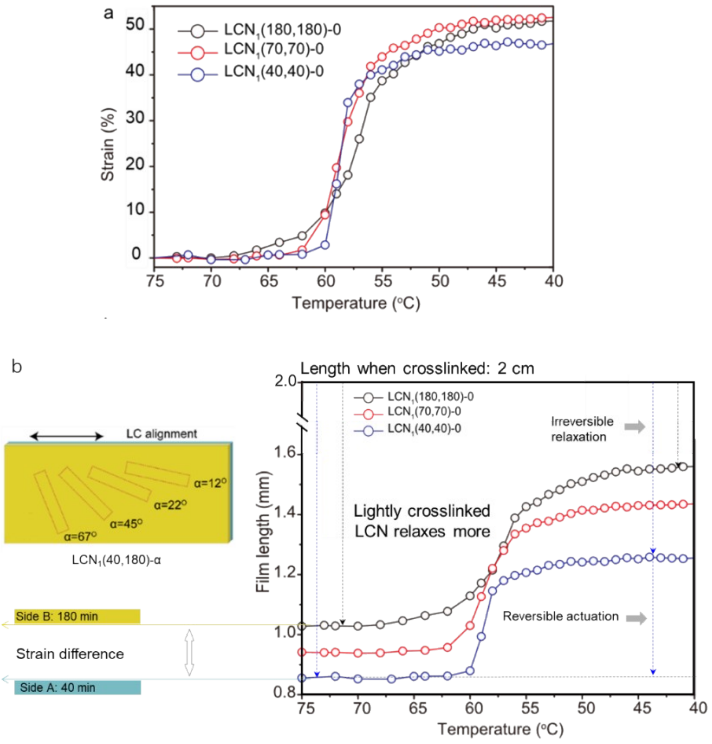

Fig. S10. (a) Strain change as a function of temperature for LCN_1(40, 40)-0, LCN_1(70, 70)-0 and LCN_1(180, 180)-0 recorded during cooling. (b) Right: Change of the absolute length of the LCN_1(40, 40)-0, LCN_1(70, 70)-0 and LCN_1(180, 180)-0 recorded during

cooling. The films during photocrosslinking process are all 2 cm. Left: Schematics showing the strain difference arising from the asymmetrically crosslinked sides, using the results in the right figure as the references.

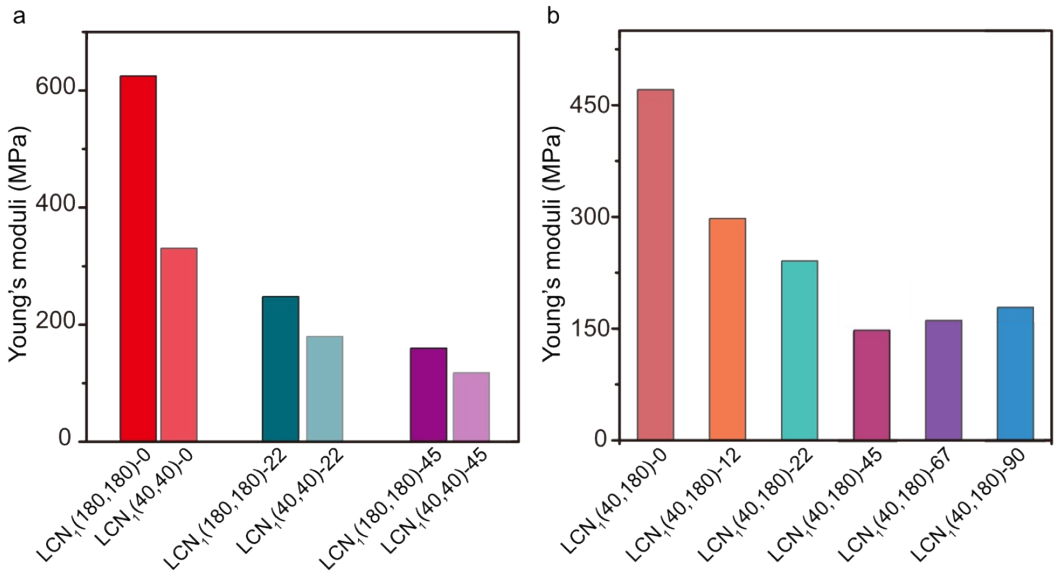

Fig. S11. Young's Modulus of (a) $LCN_1(40,40)$-α and $LCN_1(180,180)$-α strips with α=0°, 22° and 45°, and (b) $LCN_1(40, 180)$-α strips with $0° \leq \alpha \leq 90°$.

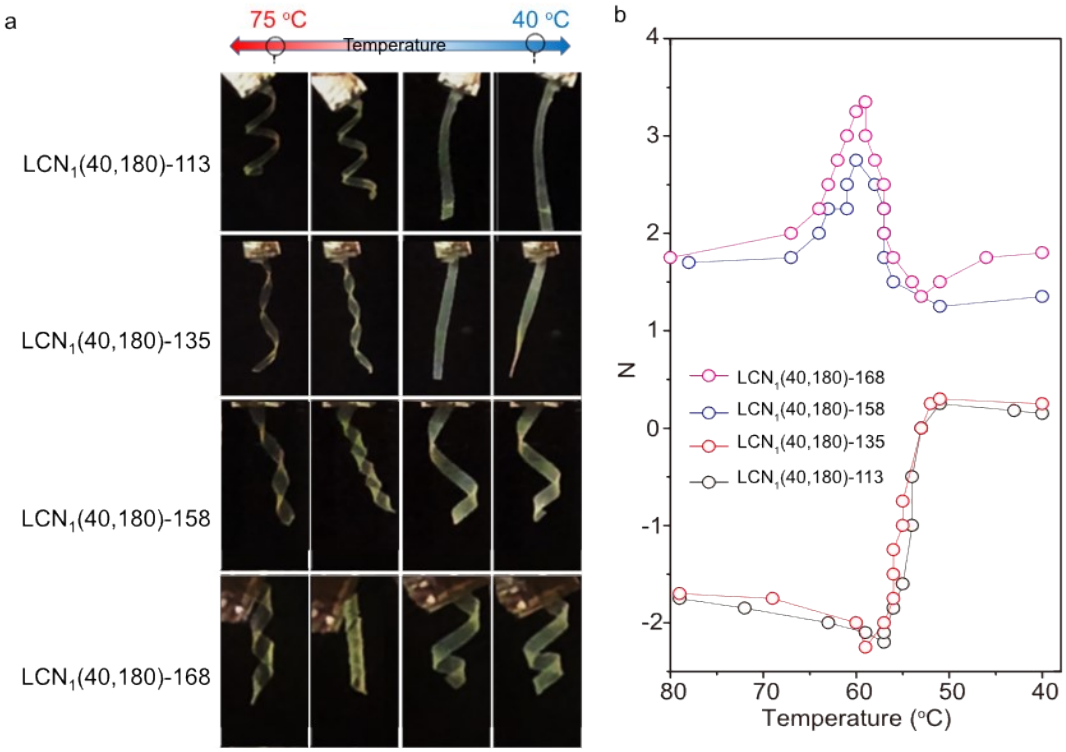

Fig. S12. (a) Images and (b) number of helical turns-temperature curves showing chiral deformation reversal of $LCN_1(40,180)$-113, $LCN_1(40,180)$-135, $LCN_1(40,180)$-158

and LCN_1(40,180)-168 strips. The helical shapes are right-handed. The dimensions of the samples are 7 (l) x 0.5 (w) x 0.07 (t) mm^3 in their maximum extended state.

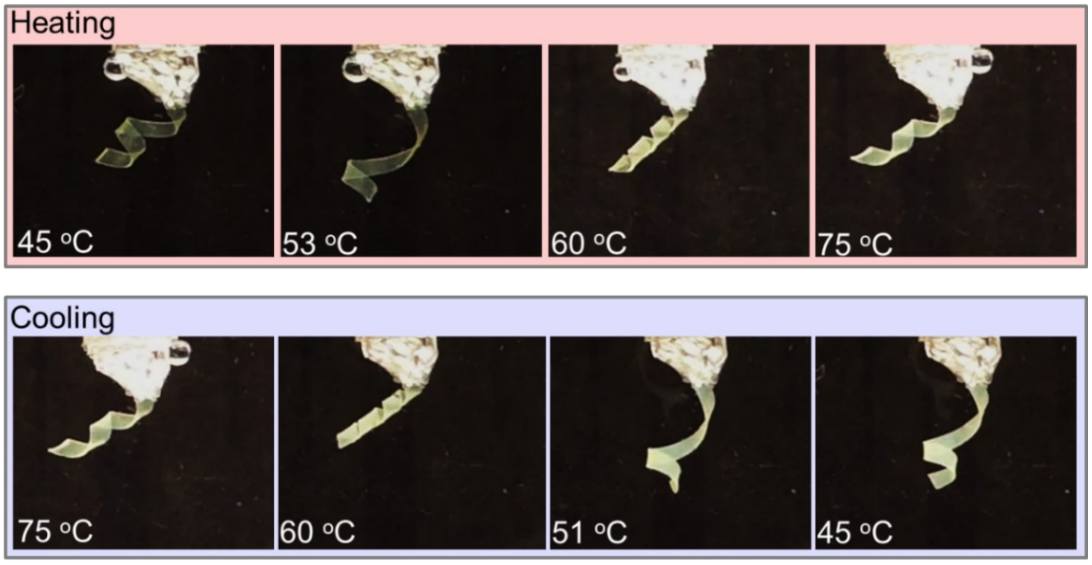

Fig. S13. Reversible deformation reversal behaviors of LCN_1(40,180)-22 strips during heating and cooling. The dimension of the sample is 7 (l) x 0.5 (w) x 0.07 (t) mm^3 in their maximum extended state.

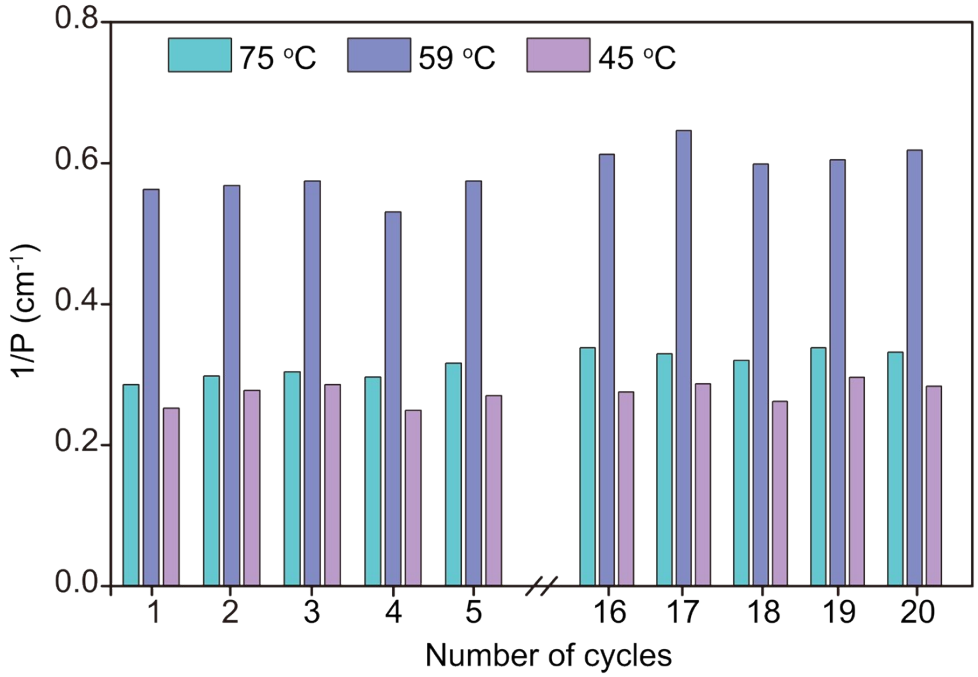

Fig. S14. The inverse of the pitches (1/P) of the LCN_1(40,180)-α strips at 75 °C, 59±1 °C and 45 °C during 20 successive cooling processes.

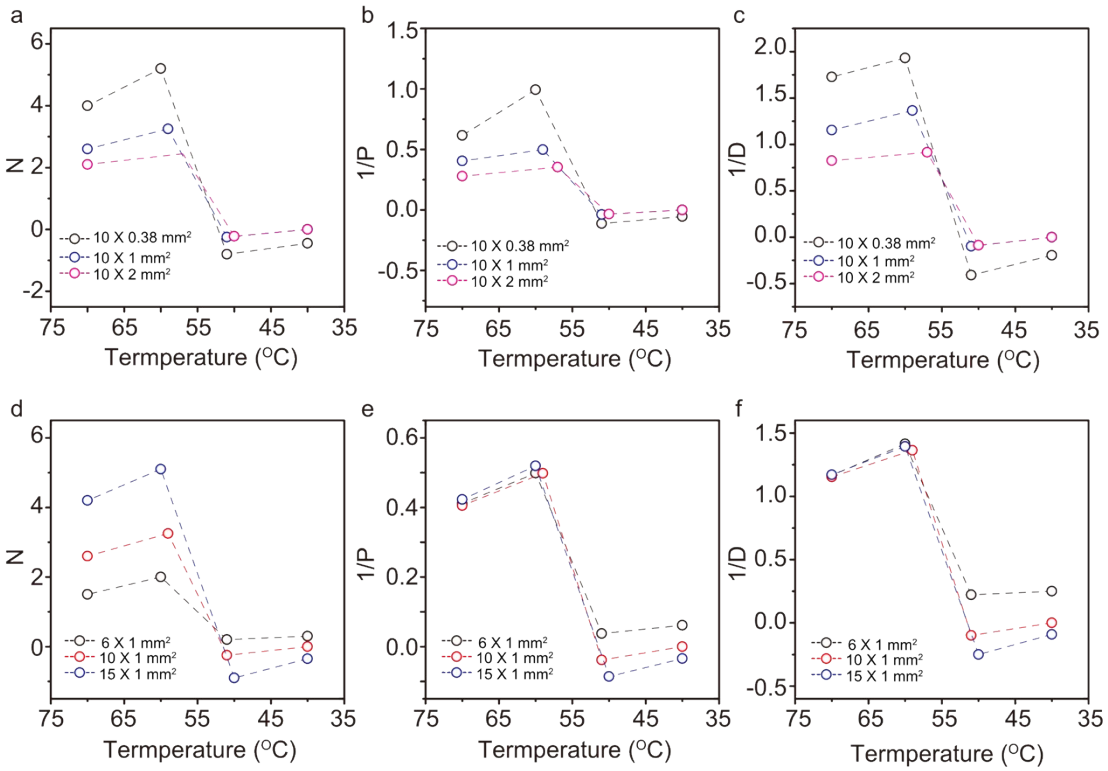

Fig. S15. Effect of width on the structural parameters of helical actuators: (a) helical turns (N), (b) the inverse of the pitches (1/P) and (c) the inverse of the diameters (1/D) of the LCN_1(40, 180)-22 strips with different widths at 75 °C, ~59 °C, ~ 51 °C and 40 °C. Note that the dash lines connecting the four data points are drawn to guide the eyes. Effect of film length on the structural parameters of helical actuators: (d) N, (e) 1/P and (f) 1/D of the LCN_1(40, 180)-22 strips with different lengths at 75 °C, ~59 °C, ~ 51 °C and 40 °C. The thickness is 0.06 mm.

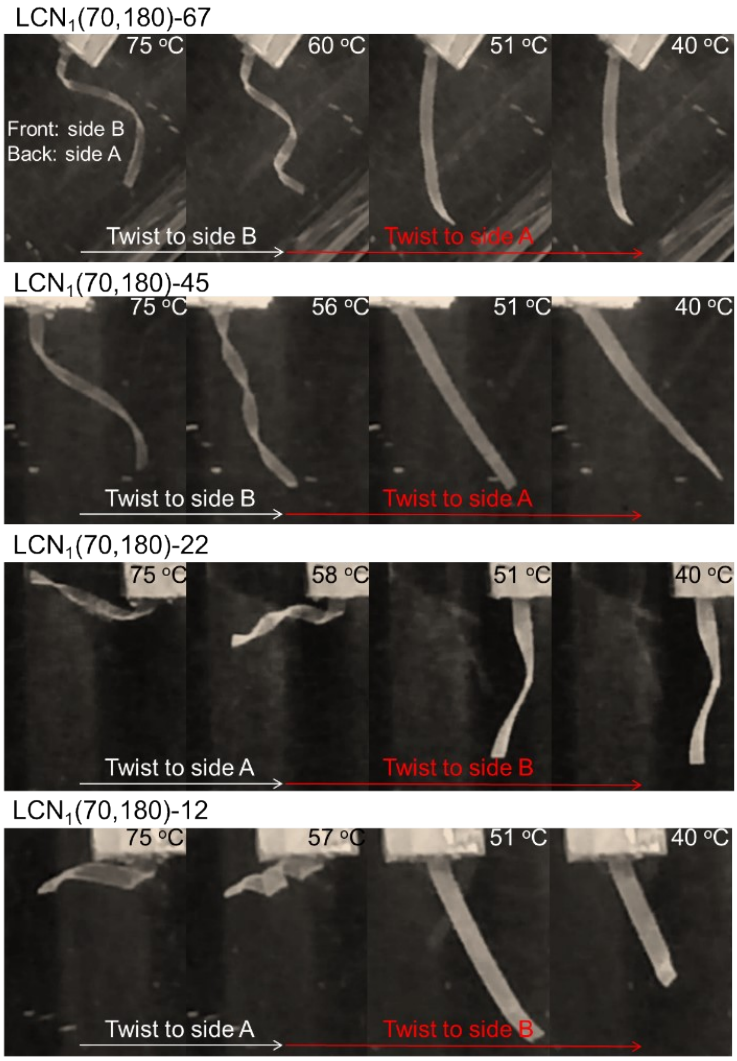

Fig. S16. Photographs showing shape changes of LC1(70,180) with different α. The dimensions of the samples are 7 (l) x 0.5 (w) x 0.07 (t) mm^3 in their maximum extended state.

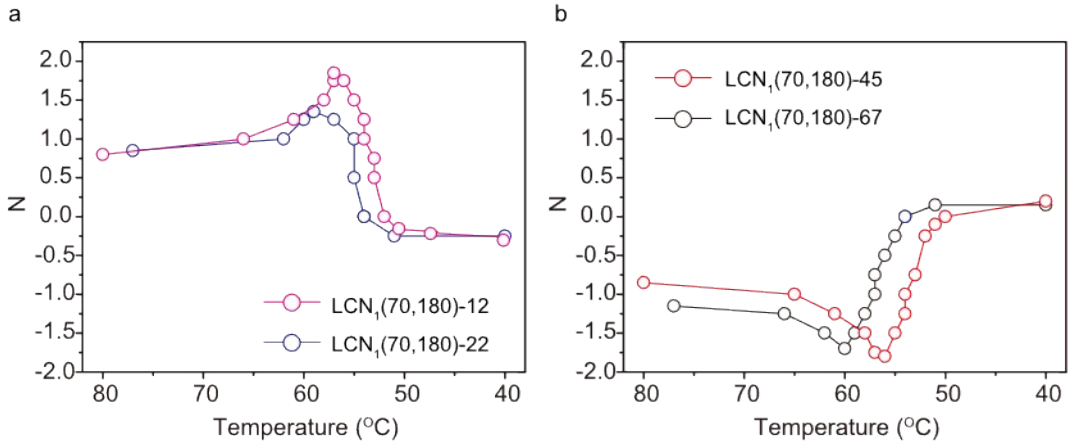

Fig. S17. Temperature dependence of the helical turns (N) for LCN_1(70, 180)-α strips during a cooling process.

Movie Captions

Movie S1

Chiral deformation-reversal behaviors of the LCN_1(40,180)-12 and LCN_1(40,180)-22 actuators with a dimension of 7 (l) x 0.5 (w) x 0.07 (t) mm^3 during cooling.

Movie S2

Two reversals of twisting direction during cooling-induced deformation process of an LCN_1(40,180)-22 actuator with a dimension of 10 (l) x 0.38 (w) x 0.06 (t) mm^3.

Movie S3

Deformation with combined features of helix-inversion and chiral deformation-reversal recorded using an LCN_2(480%,400%)-12 actuator with a dimension of 7 (l) x 0.5 (w) x 0.07 (t) mm^3 during cooling.

Supplementary references

S1. A. N. Kraskouski, V. I. Kulikouskaya, K. S. Hileuskaya, J. N. Kalatskaja, E. L. Nedved, N. A. Laman, V. E. Agabekov, *Russian Journal of Applied Chemistry,* **2020**, 93, 512-518.